1-1-1993

Angle-Resolved Photoelectron Spectrometry Of Atomic Nitrogen

S. J. Schaphorst
University of Central Florida

S. B. Whitfield
University of Central Florida

H. P. Saha
University of Central Florida

C. D. Caldwell
University of Central Florida

Yoshiro Azuma

Angle-resolved photoelectron spectrometry of atomic nitrogen

S.J. Schaphorst, S.B. Whitfield,* H.P. Saha, and C.D. Caldwell
Department of Physics, University of Central Florida, Orlando, Florida 32816-2385

Yoshiro Azuma
Argonne National Laboratory, Argonne, Illinois 60439
(Received 27 July 1992)

The relative photoionization cross section of atomic nitrogen across the $2s2p^3(^5S^o)np(^4P^e)$ autoionizing states and the β parameter over the $2s \rightarrow 3p$ and $4p$ resonances are measured using synchrotron-radiation-based photoelectron spectrometry. Results are compared with a multiconfiguration Hartree-Fock calculation. Resonance energies for autoionizing states from $n = 3$—10 are presented and compared with an earlier experiment. Values of the line-shape parameters Γ, q, and ρ^2 and discrete oscillator strengths f for the $3p$, $4p$, and $5p$ resonances are reported.

PACS numbers: 32.80.Dz, 32.80.Fb

I. INTRODUCTION

In atomic photoionization, as the photon energy is tuned across resonant transitions of a more tightly bound electron, the photoionization cross section will display autoionization structure resulting from interchannel interactions [1]. Rapid variations in the photoionization cross section are generally accompanied by fluctuations in the angular distribution of the photoelectrons due to the enhancement of electron interactions which are relatively weak in nonresonant photoionization [2]. Shapes of the autoionizing resonances reveal information on the dynamics of the photoionization process and can serve as proving grounds for theoretical models of atomic photoionization. For members of a Rydberg series of resonances in which the autoionization involves full participation of the outer electron, the line shapes are expected to share certain characteristics [3].

Experimental study of autoionization structures in open-shell atoms such as nitrogen has been restricted due to the transient nature of these reactive species. However, theoretical interest in the photoionization cross sections of nitrogen over the photon energy range from threshold at 14.55 eV to energies greater than 40 eV has been considerable [4–8]. The open-shell structure and consequent high degree of correlation among outer-shell electrons makes accurate calculations for the photoionization cross sections difficult. Nevertheless, a recent R-matrix calculation concludes that the photoionization cross section from threshold to 95 eV is now known to within a few percent [8].

The total photoionization cross section of nitrogen over a photon energy region including the $2s2p^3(^5S^o)np(^4P^e)$ Rydberg series, 17.7–20.4 eV, was measured in photoabsorption by Ehler and Weissler [9], and later by Comes and Elzer [10]. Recently, Samson and Angel [11] have recorded the photoionization cross section of nitrogen using ion spectroscopy. The first observation of the $2s2p^3(^5S^o)np(^4P^e)$ Rydberg series was made by Carroll *et al.* [12], who were able to resolve the first 12 autoionizing resonances. In a later absorption experiment the natural widths, line-shape parameters q and ρ^2, and oscillator strengths for the $2s \rightarrow 3p$ and $4p$ resonances were reported [13]. For the above experiments, atomic nitrogen was produced using discharge tubes. Alternatively, atomic nitrogen has recently been produced by laser photodissociation of nitrous oxide in a measurement of the photoelectron angular distribution from ionization of N $2p^23p(^2S^o_{1/2})$ [14].

In this paper we present a study of the nitrogen $2s2p^3(^5S^o)np(^4P^e)$ autoionizing resonances using synchrotron-radiation-based electron spectrometry. We measure the relative photoionization cross section over the $2s \rightarrow np$ resonances for $n \geq 3$. The resonance energies and quantum defects δ for states up to $n = 10$ are compared with the experimental results of Carroll *et al.* [12]. Line-shape parameters Γ, q, and ρ^2, and discrete oscillator strengths f are measured for the first three autoionizing states. Results for the $3p$ and $4p$ resonances are compared with those of Dehmer, Berkowitz, and Chupka [13]. In addition, we measured for the first time the angular distribution of photoelectrons for the $n = 3$ and $n = 4$ resonances. Results for the β value and the relative cross section are compared with those of a multiconfiguration Hartree-Fock (MCHF) calculation [15].

II. EXPERIMENT

Our electron spectrometry with synchrotron radiation studies were performed using the 4-m normal-incidence monochromator (NIM) at the Aladdin storage ring in Stoughton, Wisconsin. The electron spectrometer has been described in detail elsewhere [16, 17]. Nitrogen atoms were produced in a 2.45-GHz microwave discharge from N_2 of purity > 99.99%. The inner walls of the discharge tube were coated with phosphorous pentoxide to reduce the recombination rate on the surfaces. The resulting molecular and atomic nitrogen flowed into the

ionization chamber through an 11-mm diameter, 30-cm-long flow tube with a 5-mm diameter flow restriction at the end to maintain a pressure gradient between the discharge tube and the low-pressure ionization region. The flow tube was coated with halocarbon wax.

Spectra were normally recorded in the constant-ionic-state (CIS) mode [18]. In the CIS mode, as the photon energy is varied, the intensity of photoelectrons which leave the parent ion in the same final state is recorded. A retarding or accelerating electric field was varied with the photon energy such that the electron-energy analyzers maintained a constant pass energy. In such a way, the intensity of the photelectron peak serves as a measure of the photoionization cross section, and the resolution of the CIS spectra is determined solely by the bandpass of the monochromator. As the β parameter can be derived from partial photoionization cross sections, the CIS method is also used to determine β values by simultaneous scans at 0° and 90° with respect to the polarization vector. The current from a nickel mesh placed between the monochromator and the ionization region monitored the photon flux. Photoelectron (PE) spectra were recorded primarily to determine (1) the background contribution to the CIS measurements and (2), in cases of β measurements, the ratio of photoelectron intensities parallel and perpendicular to the polarization vector. A typical PE spectrum used a pass energy of 10.8 eV and had a resolution of nominally $\Delta E/E = 0.01$.

The 4-m NIM was equipped with a 3600-line/mm Au-coated grating. The bandpass was set to 0.16±0.01 Å, as measured from the widths of the Xe $5p^6(^1S_0) \rightarrow 5p^5(^2P_{1/2})ns'$ autoionizing resonances and the zero-order light associated with the monochromator entrance- and exit-slit settings. The wavelength was calibrated against the energies of these same Xe autoionizing resonances [19, 20] and the Ar $3s^23p^6(^1S_0) \rightarrow 3s3p^6(^2S_{1/2})np$ resonances [21]. The high β values for Xe $5p_{3/2}$ and $5p_{1/2}$ photoionization, 1.78(2) and 1.65(3), respectively, at 21.22 eV [22] allowed an accurate determination of the polarization-vector offset. Well-known β values of Xe $5p$, Kr $4p$, and Ar $3p$ photoionization at 21.22 eV [22] served as calibrations for the degree of polarization and the relative response functions of the analyzers. Ar $3p$ PE spectra at photon energies between 16.1 and 19.5 eV provided further calibrations for the degree of polarization and the response functions. The polarization was found to be essentially independent of photon-energy within this energy range and equal to 0.78 ± 0.02.

A large, approximately constant, background signal suggested the creation of metastable states of N or N_2 in the discharge. The long-lived nitrogen $2s^22p^3(^2D^o)$ and $(^2P^o)$ levels [23] lie 2.38 and 3.58 eV, respectively, above the $^4S^o$ ground state [19]. While these might be reached through collisions of the ground-state atom with electrons in the discharge tube [24, 25], similar experiments on atomic chlorine [26] gave no evidence of metastable states at 1.9 eV above the ground state. However, electronically excited metastable states of molecular nitrogen, such as the $A\,^3\Pi_u^+$ state, have been observed in discharges [24, 27]. Diffusion of such excited atomic and molecular species into the ionization region and subsequent collisions with the channeltrons produced a substantial background to the signal.

III. RESULTS AND DISCUSSION

Within the dipole approximation, the measured intensity of photoelectrons ejected from level i at an angle θ with respect to the direction of polarization satisfies the proportionality [28]

$$I(\theta)_i \propto \frac{d\sigma_i}{d\Omega} = \frac{\sigma_i}{4\pi}\left[1 + \frac{\beta_i}{4}(1 + 3p\cos 2\theta)\right]. \quad (1)$$

In this formula $d\sigma_i/d\Omega$ is the differential cross section; σ_i and β_i are, respectively, the angle-integrated cross section and anisotropy parameter, and p represents the degree of polarization of the synchrotron radiation. From Eq. (1), the anisotropy parameter can be described as a function of the ratio R_i of photoelectron intensities measured parallel and perpendicular to the direction of the polarization vector,

$$\beta_i = \frac{4(R_i - 1)}{[3p(R_i + 1) - (R_i - 1)]}. \quad (2)$$

In accord with LS coupling, photoionization of the ground N $2s^22p^3(^4S^o)$ state results in a $^4P^e$ final state for the ion plus photoelectron. The $2s2p^3(^5S^o)np(^4P^e)$ resonances can therefore only autoionize into the continuum state of the $2s^22p^2(^3P^e)$ ion plus a photoelectron, ks or kd, coupled to form a $^4P^e$ state. The total cross section σ in this energy range is therefore directly proportional to the intensity of $2p$ photoelectrons measured at the "magic" angle, $\theta_m = (1/2)\cos^{-1}(-1/3p)$, which leave the ion in the $^3P^e$ state. The "magic" angle is the angle for which the term multiplying β_i in Eq. (1) is zero.

A photoelectron spectrum of atomic and molecular nitrogen is shown in Fig. 1. The binding energy of $2p$ electrons which leave the ion in the $N^+(^3P^e)$ state is 14.55 eV [19]. Photoionization of ground-state $N_2(^1\Sigma_g^+)$ leads to $N_2{}^+(^2\Sigma_g^+)$ final ionic states with binding energies of 15.60 and 15.90 eV, corresponding to the $v = 0$ and 1

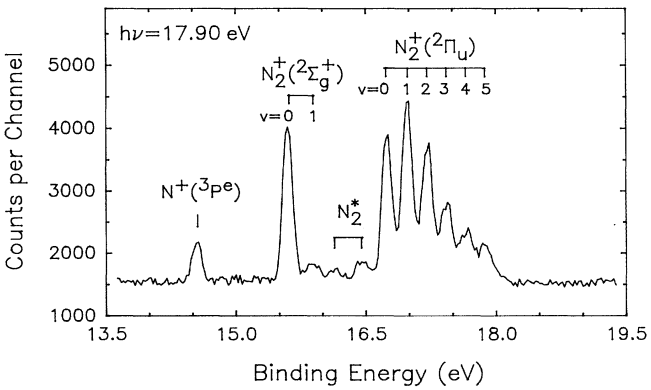

FIG. 1. Photoelectron spectra of atomic and molecular nitrogen at a photon energy of 17.90 eV. The spectrum was recorded close to the $2s \rightarrow 3p$ resonance at $\theta = 0°$ with 256 channels.

vibrational states, respectively, and to the $N_2{}^+(^2\Pi_u)$ vibrational manifold. $N_2{}^+(^2\Pi_u)$ vibrational states from $v = 0$ to 5 can be seen in Fig. 1 with binding energies from 16.74 to 17.86 eV [29]. If LS coupling rules are broken, photoionization of atomic nitrogen could lead to a photoelectron peak at 16.45 eV associated with the $2s^22p^2(^1D^e)$ final ionic state [19]; however, a CIS spectrum of the peak at 16.46 eV binding energy over the N $2s2p^3(^5S^o)np$ resonances revealed no autoionizing structure. The small peaks labeled N_2^* at 16.46 and 16.13 eV are believed to result from transitions of the vibrationally excited $v = 1$ and $v = 2$ states of neutral $N_2(^1\Sigma_g^+)$, respectively, to the $N_2{}^+(^2\Pi_u, v = 0)$ ionic state plus photoelectron [30]. The large background signal in Fig. 1, about 1550 counts per channel, is attributed to electronically excited metastable atomic and/or molecular species striking the channeltrons.

With an electron spectrometer resolution of $\simeq$ 130 meV the splitting of the $^3P_0^e$ and $^3P_1^e$ photopeaks and the $^3P_1^e$ and $^3P_2^e$ photopeaks, 6.1 meV and 16.3 meV, respectively, could not be resolved. CIS spectra were therefore limited to recording the sum of photoelectrons leaving the parent ion in the $J = 0$, 1, and 2 states. Since LS coupling is expected to describe the nitrogen states accurately, CIS spectra of the $N^+(^3P^e)$ photopeak in the photon-energy region of the $2s2p^3(^5S^o)np(^4P^e)$ resonances measure the total photoionization cross section of atomic nitrogen, subject to the calibration of the absolute detection efficiency.

The photoionization cross section across the $2s \rightarrow np$ autoionizing resonances for $n \geq 3$ is shown in Fig. 2. The spectrum was taken with a 5-meV stepsize. The cross section has been normalized to our MCHF results described in Sec. IV and the Appendix. Resonance energies and corresponding quantum-defect parameters for np states

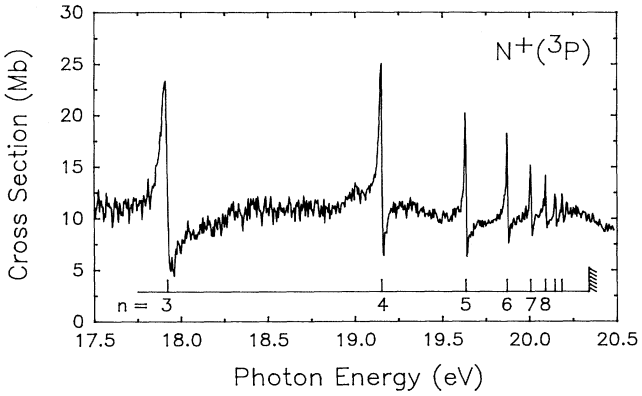

FIG. 2. Photoionization cross section of atomic nitrogen across the N $2s^22p^3(^4S) \rightarrow 2s2p^3np$ autoionizing resonances for $n \geq 3$. The spectrum was recorded in a CIS scan with a constant bandpass of 0.16 Å and a 5-meV/channel stepwidth at $\theta = 57.65°$. Absolute values are determined by normalization to the MCHF result at 18.6 eV.

from $n = 3$ to 10 are listed in Table I. The resonance energies have been determined by fitting the data with a Shore function [31] convoluted with a Gaussian of 0.16 Å full width at half maximum to account for the energy width of 4.7 meV at $\hbar\omega = 19.0$ eV of the incident photon beam. The shape of the monochromatized photon beam was verified by scanning the zero-order profile and was found to remain essentially Gaussian over two orders of magnitude in the beam width. The Shore and Fano [1] profiles are of the same functional form, and fitting parameters for each function can be related. To compare our results with an earlier paper [13], we report the lineshape parameters ρ^2 and q of a Fano profile for the $3p$, $4p$, and $5p$ resonances, given by [1]

TABLE I. Energies and quantum defect parameters δ for the nitrogen $2s^23p^3(^4S^o) \rightarrow 2s2p^3(^5S^o)np(^4P^e)$ series. The uncertainty of $\pm$ 7 meV in the calibration of the photon energy is not included in column four.

	Theory		Experiment				
	Present work		Present work		Carroll *et al.*[a]		
					E (eV)		δ
np	E (eV)	δ	E(eV)	δ	(1)	(2)	
$3p$	17.9114	0.654	17.9213(10)	0.628	17.8985	17.9073	0.63
$4p$	19.1892	0.624	19.1529(2)	0.613	19.1482	19.1510	0.61
$5p$	19.6707	0.629	19.6333(2)	0.609	19.6296	19.6308	0.60
$6p$	19.9120	0.624	19.8710(2)	0.608	19.8675		0.59
$7p$	20.0480	0.625	20.0062(3)	0.606	20.0025		0.58
$8p$	20.1330	0.620	20.0904(4)	0.602	20.0862		0.58
$9p$	20.1891	0.619	20.1450(6)	0.626	20.1397		0.62
$10p$			20.1848(6)	0.607	20.1811		0.55
∞	20.3828		20.3388(2)		20.335(2)	[20.3971[b]]	

[a]Reference [12]. Column (1) is the energy, as reported, of the absorption peak. The resonance energy in column (2) is found by taking the difference in energy between the resonance energy and the peak energy as $\Gamma/2q$.

[b]Spectroscopic value [19].

$$\sigma(\epsilon) = \sigma_c \left[\frac{(q+\epsilon)^2}{1+\epsilon^2} \rho^2 + (1-\rho^2) \right] \quad (3)$$

where

$$\epsilon = \frac{(\hbar\omega - E_r)}{\Gamma/2}, \quad (4)$$

E_r is the resonance energy, Γ is the natural width of the autoionizing state, and σ_c represents the cross section for photon energies outside of the resonance region, or where $\epsilon >> 1$ and q [32].

In Table I the present experimental results are compared with those of Carroll *et al.* [12] and the MCHF calculation described in Sec. IV. In addition to the statistical uncertainty of the resonance energies shown in column four, there is an uncertainty in the photon-energy calibration of ± 7 meV. The energies reported by Carroll *et al.* and shown in column six refer to the peak of the cross section and therefore depend on the bandwidth of the photon source. With no instrumental broadening of the Fano profile, the maximum of the cross section will occur at an energy of $E_{np} + \Gamma/2q$. Although Carroll *et al.* give no bandwidth for the photon energy, we determine from an analysis of their spectra a value < 2 meV. Thus, the difference in energy between peak heights of the convoluted and the unconvoluted Fano profiles should be negligible for the $3p$, $4p$, and $5p$ resonances. The adjusted resonance energies, employing a value of $q = -1.7$, are listed in column seven of Table I. Although our $3p$ resonance energy disagrees with the value reported by Carroll *et al.* by 14 meV, energies of the higher np resonances agree within 5 meV.

Quantum defect parameters δ_{np} were determined from the relation

$$E_\infty - E_{np} = \frac{1}{(n-\delta_{np})^2}, \quad (5)$$

where the energies E_{np} are in rydbergs. The quantum defect parameter δ_{np} and the continuum energy E_∞ were found from a best fit of $\delta_{np} = f(E_\infty - E_{np})$ to a first-order polynomial in $E_\infty - E_{np}$ [33]. The discrete oscillator strengths for the resonances were determined from the expression [3]

$$f = \frac{mc^2}{2e^2} \sigma_0 \rho^2 \Gamma q^2 , \quad (6)$$

where e and m are the charge and mass of the electron, respectively, c is the speed of light, and σ_0 is the cross section of the underlying continuum. To put the oscillator strengths on an absolute scale, the cross section σ_0 has been set to 11 Mb, in agreement with our MCHF calculation at a photon energy of 18.6 eV. A recent R-matrix calculation of Bell and Berrington [8] presents a total cross section in this energy region which appears approximately 25% higher than our calculated theoretical result. Samson and Angel [11] measured values which are generally 10–15 % lower than the Bell and Berrington calculation in the region of the $2s \rightarrow np$ resonances. However, Bell and Berrington argue that their calculation of the photoionization cross sections and the measurements of Samson and Angel would agree within a few percent if the normalization of the experimental data were to employ the oscillator strength values which Bell and Berrington calculated. The total photoionization cross-section measurements of Ehler and Weissler [9] lie within a few percent of the theoretical results of Bell and Berrington. Comes and Elzer [10], however, reported a cross section of about 9 Mb near the $3p$ and $4p$ resonances.

The total cross section across the $3p$ and $4p$ resonances is shown in Figs. 3(a) and 4(a). The spectra were taken with a 2-meV step size. The long-dashed lines indicate the resonance energies E_{np} as described by Eq. (4). The solid lines in Figs. 3(a) and 4(a) are χ^2 fits to the data with the fitting function a convoluted Shore profile as described above.

Values of Γ, q, ρ^2, and f, as described by Eqs.(3), (4), and (6) are listed in Table II for the $3p$, $4p$, and $5p$ resonances. The present results for the $3p$ and $4p$ resonances agree with those of Dehmer *et al.* within the experimental errors. For comparison, the oscillator strengths of Dehmer, Berkowitz, and Chupka [13] have been normalized to a continuum cross section of 11 Mb. Reported values support the contention that members of a Rydberg series of autoionizing resonances with an approximately constant quantum defect δ are described by nearly equal values of q and ρ^2 [32]. The natural widths for the $3p$, $4p$, and $5p$ resonances are seen to be approximately proportional to $(n-\delta)^{-3}$.

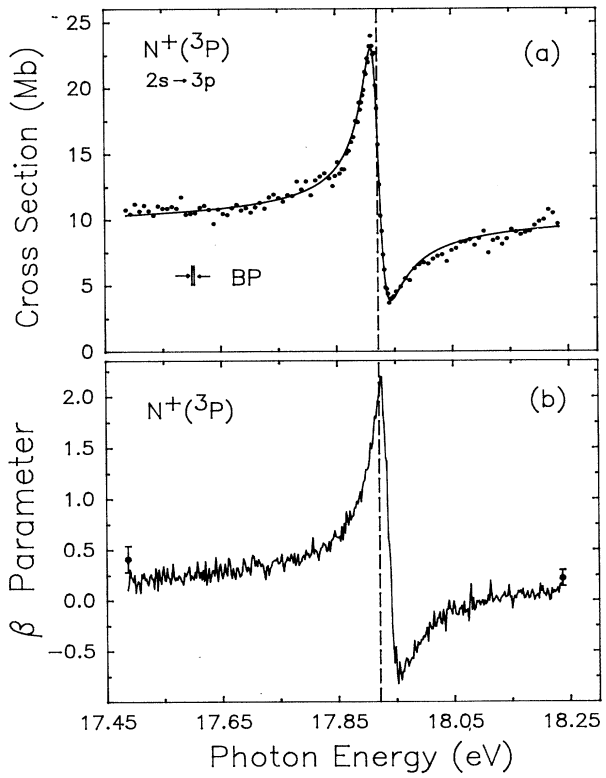

FIG. 3. Photoionization cross section and β parameter for atomic nitrogen across the N $2s^2 2p^3 (^4S) \rightarrow 2s2p^3 3p$ autoionizing resonance. The dashed lines indicate the resonance energy positions. The solid lines represent a χ^2 fit to the data.

TABLE II. Widths, line-shape parameters, and oscillator strengths for the nitrogen $2s^2 2p^3(^4S) \rightarrow 2s2p^3(^5S^o)np(^4P^e)$ resonances for $n = 3$, 4, and 5.

	3p		4p		5p
	Present work	Dehmer *et al.*[a]	Present work	Dehmer *et al.*[a]	Present work
Γ (meV)	29.8(6)	27.5(3.0)	9.4(3)	10(3)	4.4(3)
Γn^{*3}	0.398(8)		0.365(12)		0.373(25)
q	-1.60(24)	-1.7(1)	-1.70(7)		-1.9(3)
ρ^2	0.59(8)	0.51(4)	0.56(7)	0.58(15)	0.65(15)
f (units of 10^3)	6.2(6)	6.4(1.2)[b]	2.4(5)	2.6(1.1)[b]	1.6(6)

[a]Reference [13].
[b]Normalized to our MCHF value of $\sigma_0 = 11$ Mb as discussed in Sec. III.

The β parameter for $2p$ photoionization across the $2s \rightarrow 3p$ and $2s \rightarrow 4p$ resonances is shown in Figs. 3(b) and 4(b). PE spectra, given as filled circles, provide a normalization for the CIS spectra at the energy end points of the CIS scan. These β values, and their associated errors, are calculated from the ratio of the $N^+(^3P^e)$ integrated photopeaks measured parallel and perpendicular to the polarization direction, according to Eq. (2). The β values from the CIS measurements derive from the ratio of intensities measured at 0° and 90°, following subtraction of the metastable background. Errors associated with the CIS β values result from (1) the statistical error of the measured intensities at 0° and 90°, (2) uncertainty in the polarization and the relative response functions of the analyzers, and (3) uncertainty in the background contributions. Long-term drifts in the background levels produced by fluctuations in the discharge complicated the background subtraction. With an off-resonance signal-to-background ratio of typically 1:2, deviations of the background contribution in time from its assumed linear behavior significantly affect the β values derived from CIS spectra. These sources of error account for the β values above 2 at the maxima of the resonances and the differences between the β values determined by the PE and CIS spectra in the tails of the $2s \rightarrow 3p$ spectrum of Fig. 3(b). The effect of the $2s$-subshell interchannel interaction on β is striking in the resonance regions and results in a variation of the anisotropy parameter almost over its entire allowed range, +2 to −1.

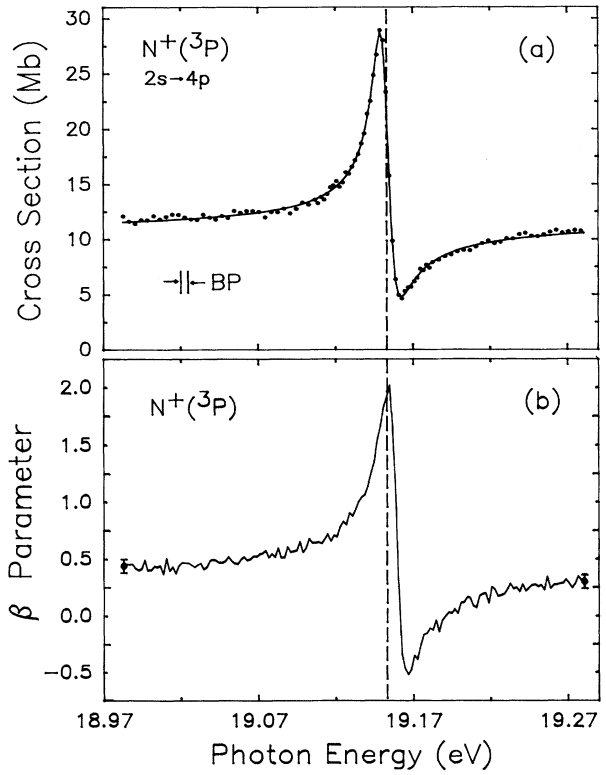

FIG. 4. Photoionization cross section and β parameter for atomic nitrogen across the N $2s^2 2p^3(^4S) \rightarrow 2s2p^3 4p$ autoionizing resonance. The dashed lines indicate the resonance energy positions. The solid lines represent a χ^2 fit to the data.

IV. THEORY

Recently the MCHF method has been shown to produce accurate results for atomic photoionization processes [34–36]. In connection with the experimental work we performed a theoretical study of the $2p$ photoionization of the ground-state nitrogen atom using the MCHF method. As mentioned in our previous work, the MCHF method takes into account electron-correlation effects very efficiently in an *ab initio* manner through the configuration-interaction procedure. Thus, it should be an excellent tool for the study of nitrogen, as nitrogen is an open-shell atom and electron correlation must be considered very accurately.

The anisotropy parameter β_{nl}, as described by Eq. (1), was calculated using the Cooper-Zare model [37],

$$\beta_{nl}(\omega) = \frac{l(l-1)T_-^2(\omega) + (l+1)(l+2)T_+^2(\omega) - 6l(l+1)T_-(\omega)T_+(\omega)\cos(\xi_+ - \xi_-)}{(2l+1)[lT_-^2(\omega) + (l+1)T_+^2(\omega)]} \quad (7)$$

where $T_-(\omega)$ and $T_+(\omega)$ are the radial parts of the dipole matrix element corresponding to the $l-1$ and $l+1$ channels, respectively. Similarly, ξ_- and ξ_+ are the phase shifts of the $l-1$ and $l+1$ channel, respectively. Details of the MCHF method as applied to photoionization are described in the Appendix. We focus on the process

$$\hbar\omega + \mathrm{N}\ 2s^2 2p^3(^4S^o) \rightarrow \mathrm{N}^+\ 2s^2 2p^2(^3P^e) + e^-.$$

In order to study the autoionization resonances, particular attention was paid to the single- and double-electron excitations in the MCHF calculation for the initial- and final-state wave functions.

The initial ground state of nitrogen consists of 18 configurations:

$$\{2s^2 2p^3, 2s2p^3 3s, 2s2p^3 3d, 2s^2 2p^2 3p, 2s2p^2 3s3p,$$

$$2s2p^2 3p3d, 2p^4 3p, 2s^2 2p3p^2, 2s^2 2p3d^2, 2p^3 3s^2,$$

$$2p^3 3d^2\}^4 S^o.$$

The MCHF wave-function expansion for the ground state of the N^+ ion was over a set of nine configuration states coupled to form a $^3P^e$ term:

$$\{2s^2 2p^2, 2p^4, 2s2p^2 3s, 2s2p^2 3d, 2s^2 3d^2, 2p^2 3d^2\}^3 P^e.$$

The final-state continuum-wave-function configuration adopted in the present study is composed of the 43 terms arising from the configurations formed by coupling the nine ionic core configurations with each continuum kd or ks wave function plus the 34 bound configurations,

$$\{\ 2s^2 2p^2 3s, 2p^4 3s, 2s^2 2p^2 3d, 2p^4 3d, 2s2p^3 3p, 2s2p^3 4p,$$
$$2s2p^2 3s^2 2s2p^2 3s3d, 2s2p^2 3d^2, 2p^2 3s3d^2, 2p^2 3d^3,$$
$$2s^2 3d^3, 2s^2 3s3d^2\}^4 P^e.$$

In each case the $1s$, $2s$, and $2p$ orbitals are those obtained from the HF N^+ $2s^2 2p^2(^3P^e)$ ionic core state calculation. For the final-state wave functions, the $3p$ and $4p$ orbitals are obtained from the HF calculation of $2s2p^3 np(^4P^e)$ states with the $1s$, $2s$, and $2p$ orbitals the same as above. Other orbitals were optimized along with the continuum orbital at each photon energy.

The theoretical and experimental resonance energies for the higher Rydberg states up to $9p$ are compared in Table I. The MCHF resonance energies fall 10 meV below and 36 meV above the experimentally determined $3p$ and $4p$ energies, respectively. The theoretical value for the $2s2p^3(^5S^o)$ threshold energy lies 44 meV above the experimental value. The calculated threshold energy for the $2s^2 2p^2(^3P^e)$ state of 14.532 eV agrees well with a spectroscopic value of 14.55 eV [19].

The theoretical results for the cross section across the $3p$ and $4p$ resonances are given in Fig. 5 for both the length and velocity forms. The good overall agreement between the two calculations attests to the accuracy of the wave functions. Also given in Fig. 5 are the experimental results for comparison. The experimentally determined relative cross section has been normalized to the average of the length and velocity calculations at 18.6 eV. The influence of the bandpass has been removed by the fitting procedure as described in Sec. III. Thus, the experimental results are to be compared directly with the theoretical results. Although the profiles of the resonances are qualitatively described by the theory, the theoretical widths largely underestimate the experimental widths. The peaks of the theoretical cross sections for the $3p$ and $4p$ resonances exceed the experimental results by factors of 6.4 and 3.3, respectively. We note that this is a common feature of calculations and reflects the fact that the theoretical approach does not include all possible configurations and the accompanying channels for decay.

A comparison between the theoretical calculations of β in the length and velocity gauges and the experimental results is shown in Fig. 6. A qualitative agreement between theory and experiment for the variation in β across the $3p$ and $4p$ resonances is demonstrated in Fig. 6. The theoretical anisotropy parameter extends over the range $+2$ to -1 in the region of the resonances. The variation of β to values below zero and down to -1, resulting in a $\sin^2\theta$ photoelectron distribution, can be attributed to the interference of the ks and kd continua as described by the third term in the numerator of Eq. (7). Within the angular-momentum transfer model of Dill and Fano [38], LS-coupling rules allow only parity-favored transitions

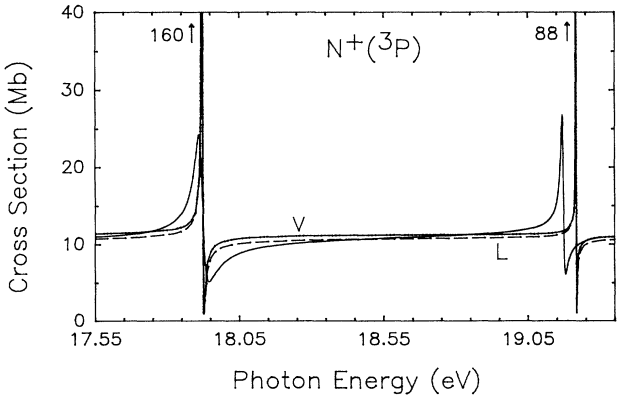

FIG. 5. Comparison of theoretical and experimental photoionization cross sections of atomic nitrogen across the $3p$ and $4p$ resonances. Results from the length and velocity gauges are indicated by L (dashed line) and V (dash-dotted line). The theoretical cross sections extend to 160 Mb and 88 Mb in the regions of the $3p$ and $4p$ resonances, respectively. The solid line represents the unconvoluted experimental data.

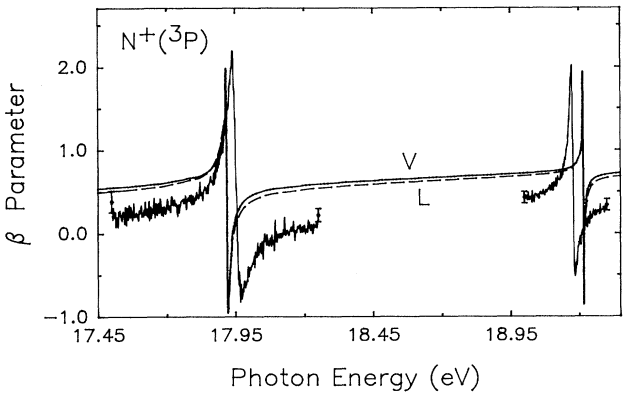

FIG. 6. Comparison of theoretical and experimental values for the β parameter of atomic nitrogen across the $3p$ and $4p$ resonances. Results from the length and velocity gauges are indicated by L (dashed line) and V (dash-dotted line). The solid lines are the experimental results.

from the $^4S^o$ ground state of nitrogen to the $2s^22p^2(^3P^e)$ ionic state. Parity-favored transitions are described by the relation $(-1)^{j_t} = \pi_0\pi_c$ in which π_0 and π_c represent the parity of the inital atomic and final ionic states, respectively, and j_t is the angular momentum transferred to the ion. Manson and Starace [39] noted that j_t can assume only one value for cases in which the orbital angular momentum of the initial-state atom or final-state ion is zero. In the case of nitrogen, parity-unfavored transitions, which result in values of $\beta = -1$ and for which $-(-1)^{j_t} = \pi_0\pi_c$ [38], are therefore not responsible for the excursions of β below zero. In regions outside of the $3p$ and $4p$ resonances, both the theoretical and experimental β parameters display a gradual rise as the photon energy increases; however, the theoretical values are consistently higher than the experimental results.

V. CONCLUSIONS

The photoionization cross section for nitrogen over the $2s2p^3(^5S^o)np(^4P^e)$ Rydberg series and the β parameter across the $2s \rightarrow 3p$ and $4p$ resonances have been measured with synchrotron-radiation-based electron spectrometry. Qualitative agreement between the experimental results and our MCHF calculation for the photoionization cross section and β parameter is found. The resonance energies for the $2s \rightarrow np$ autoionizing states from $n = 3$ to 10 are reported and compared with the results of our MCHF calculation and an earlier experiment. Natural widths Γ, line-shape parameters q and ρ^2, and discrete oscillator strengths f have been measured for the three lowest members of the Rydberg series. Comparison of the $3p$ and $4p$ line-shape parameters against previous photoabsorption results show good agreement. The near equality of the parameters q and ρ^2 is demonstrated for the $3p$, $4p$, and $5p$ resonances.

ACKNOWLEDGMENTS

We thank M.O. Krause for many useful discussions and C.A. de Lange for the use of the discharge tube. This work was supported by the National Science Foundation under Grants No. PHY-8907286 and No. PHY-9007884. Y. A. also acknowledges support from the Argonne National Laboratory under DOE Contract No. W-31-109-ENG-38. The Synchrotron Radiation Center is supported by the National Science Foundation under Grant No. DMR-8821625.

APPENDIX: MCHF THEORY

The photoionization cross section for absorbing a photon of energy $\hbar\omega$ from an initial state i to a final state f is given by

$$\sigma(\omega) = 4\pi^2\alpha a_0^2\omega \sum_{f,m} |\langle\Psi_f|T|\Psi_i\rangle|^2 , \tag{A1}$$

where α is the fine structure constant and a_0 is the mean radius of the first Bohr orbital of the hydrogen atom. The summation runs over all of the final configurations and all magnetic quantum numbers. The length and velocity forms of the dipole transition operator T are

$$T_l = \sum_{j=1}^{n} z_j \tag{A2}$$

and

$$T_v = \sum_{j=1}^{n} (i\omega)^{-1} \frac{d}{dz_j} . \tag{A3}$$

The initial- and final-state wave functions Ψ_i and Ψ_f are found to be exact solutions of the same Hamiltonian if the length and velocity forms of the cross section are identical.

The MCHF wave function for the final continuum state with energy E, label γ, and term LS is written in the form

$$\Psi_f^{N+1}(\gamma LS) = \Psi_c^N(L_cS_c)\phi_{kl} + \sum_{i=1}^{m} c_i\Phi^{N+1}(\gamma_i LS) , \tag{A4}$$

where the first term is an antisymmetrized product of an N-electron correlated wave function, $\Psi_c^N(L_cS_c)$, of angular momenta L_c and S_c, and a single-electron continuum wave function, ϕ_{kl}, of linear momentum k and orbital angular momentum l, coupled to produce an $(N+1)$-electron wave function of angular momenta L and S. The second term is a linear combination of $(N+1)$-electron bound-state wave functions, $\Phi^{N+1}(\gamma_i LS)$, having the same angular momenta L and S.

The ionic core wave function can be written in the form

$$\Psi_c^N(L_cS_c) = \sum_{j=1}^{m_c} a_j\Phi^N(\gamma_j L_cS_c) \tag{A5}$$

where $\Phi^N(\gamma_j L_cS_c)$ are bound eigenstates of ionic core configuration γ_j with angular momenta L_c and S_c, and the a_j are mixing coefficients. A separate MCHF calculation determines the mixing coefficients a_j and the set of bound radial functions $P_j(r)$, $j = 1, 2, ..., N_c$ which describe the ionic core wave function. All the radial func-

tions describing the core are assumed to be fixed along with the coefficients a_j in the calculation of the final-state continuum wave function.

The bound-state wave functions $\Phi^{N+1}(\gamma_j LS)$ of Eq. (A4) are included to allow for electron-correlation effects. The coefficients c_i and a set of radial functions $P_i(r)$, $i = 1, 2, ..., N_f$ describing the bound and continuum orbitals are determined variationally by solving a set of coupled integro-differential equations in an iterative method as described in detail in an earlier paper [15].

* Present address: Fritz-Haber-Institut der Max-Planck-Gessellschaft, D-1000 Berlin 33, Germany.

[1] U. Fano, Phys. Rev. **124**, 1866 (1961).
[2] D. Dill, Phys. Rev. A **7**, 1976 (1973).
[3] U. Fano and J. W. Cooper, Rev. Mod. Phys. **40**, 441 (1968).
[4] R.J.W. Henry, J. Chem. Phys. **44**, 4357 (1966).
[5] R.J.W. Henry, J. Chem. Phys. **48**, 3635 (1968).
[6] J.U. Koppel, J. Chem. Phys. **55**, 123 (1971).
[7] M. Le Dourneuf, Vo Ky Lan, and A. Hibbert, J. Phys. B **9**, L359 (1976).
[8] K.L. Bell and K.A. Berrington, J. Phys. B **24**, 933 (1991).
[9] A.W. Ehler and G.L. Weissler, J. Opt. Soc. Am **45**, 1035 (1955).
[10] F.J. Comes and A. Elzer, Phys. Lett. **25A**, 334 (1967); Z. Naturforsch. **23A**, 133 (1968).
[11] J.A.R. Samson and G.C. Angel, Phys. Rev. A. **42**, 1307 (1990).
[12] P.K. Carroll, R.E. Huffman, J.C. Larrabee, and Y. Tanaka, Astrophys. J. **146**, 553 (1966).
[13] P.M. Dehmer, J. Berkowitz, and W.A. Chupka, J. Chem. Phys. **60**, 2676 (1974).
[14] S.T. Pratt, J.L. Dehmer, and P.M. Dehmer, Phys. Rev. A **36**, 1702 (1987).
[15] H.P. Saha, Phys. Rev. A **39**, 628 (1989).
[16] M.O. Krause, T.A. Carlson, and P.R. Woodruff, Phys. Rev. A **24**, 1374 (1981).
[17] M.O. Krause, T.A. Carlson, and A. Fahlman, Phys. Rev. A **30**, 1316 (1984).
[18] M.O. Krause, F. Cerrina, and A. Fahlman, Phys. Rev. Lett. **50**, 1118 (1983).
[19] C.E. Moore, *Selected Tables of Atomic Spectra*, Natl. Bur. Stand. Ref. Data Ser., Natl. Bur. Stand. (U.S.) Circ. No. 3 (U.S. GPO, Washington, DC, 1976), Sec. 7.
[20] K. Yoshino and D.E. Freeman, J. Opt. Soc. Am. B **2**, 1272 (1985).
[21] R.P. Madden, D.L. Ederer, and K. Codling, Phys. Rev. **177**, 136 (1969).
[22] J. Kreile and A. Schweig, J. Electron Spectrosc. Relat. Phenom. **20**, 191 (1980).
[23] W.L. Wiese, M.W. Smith, and B.M. Glennon, *Atomic Transition Probabilities*, Natl. Stand. Ref. Data Ser. Natl. Bur. Stand. (U.S.) Circ. No. 4 (U.S. GPO, Washington, DC, 1966).
[24] See, for example, F. Kaufman, Adv. Chem. Ser. **80**, 29 (1969); or R.A. Young and G.A. St. John, *ibid.* **80**, 105 (1969).
[25] W.T. Rawlins, M.E. Fraser, and S.M. Miller, J. Chem. Phys. **93**, 1097 (1989).
[26] P. van der Meulen, M.O. Krause, C.D. Caldwell, S.B. Whitfield, and C.A. de Lange, J. Phys. B **24**, L573 (1991).
[27] A.G. Engelhardt, A.V. Phelps, and C.G. Risk, Phys. Rev. **135**, A1566 (1964).
[28] M.O. Krause, in *Synchrotron Radiation Research*, edited by H. Winick and S. Doniach (Plenum, New York, 1980), p. 101; Phys. Rev. A **30**, 1316 (1984).
[29] J.B. West, K. Codling, A.C. Parr, D.L. Ederer, B.E. Cole, R. Stockbauerr, and J.L. Dehmer, J. Phys. B **14**, 1791 (1981).
[30] H. Van Lonkhuyzen, Chem. Phys. Lett. **107**, 420 (1984).
[31] B. W. Shore, J. Opt. Soc. Am. **57**, 881 (1967).
[32] U. Fano and J.W. Cooper, Phys. Rev. **137**, A1364 (1965).
[33] M.J. Seaton, Rep. Prog. Phys. **46**, 167 (1983).
[34] H.P. Saha, Phys. Rev. A **39**, 2456 (1989).
[35] H.P. Saha and C.D. Caldwell, Phys. Rev. A **40**, 7020 (1989).
[36] H.P. Saha, Phys. Rev. A **41**, 174 (1990).
[37] J. Cooper and R.N. Zare, in *Lectures in Theoretical Physics*, edited by S. Geltman, K. Mahanthappa, and W. Britten (Gordon and Breach, New York, 1969), Vol. 11e, p. 317.
[38] D. Dill and U. Fano, Phys. Rev. Lett. **29**, 1203 (1972).
[39] S.T. Manson and A.F. Starace, Rev. Mod. Phys. **54**, 38 (1982).